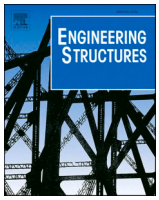
Engineering Structures 258 (2022) 114149



Contents lists available at ScienceDirect

Engineering Structures

journal homepage: www.elsevier.com/locate/engstruct





Flexural strength recovery of RC one-way slabs having cut-outs using NSM-SHCC plates

Abd-Elhakim A. Khalil, Ahmed M. Atta, Ali Hassan *, Ahmed H. Abd-Elaaty

Structural Engineering Dept, Faculty of Engineering, Tanta University, Tanta, Egypt

ARTICLE INFO

Keywords:
Strengthening
Flexure
Concrete
Slabs
Cut-outs
Opening
Strain Hardening Cementitious Composites (SHCC)

ABSTRACT

Creating a cut-out in an existing Reinforced Concrete (RC) slab became a common practice to allow passing facility services. This cut-out interrupts the loading trajectories resulting in the existence of weak points. Thus, the ultimate capacity of such slab including cut-out decreases with the increase of the size of the opening. In this paper, a new technique based on near-surface mounted has been employed using precast plates made of Strain-Hardening Cementitious Composites (SHCC). These SHCC plates were designed to compensate the cut reinforcement due to cut-out. The used plates had three different widths; 100, 200 and 300 mm, while their thickness was kept constant at 20 mm. One reference slab without cut-out, in addition to, nine damaged slabs with central cut-outs, were prepared and tested under incremental static loading. The tested slabs have the same dimensions; thickness = 140, effective depth = 120 mm, width = 1200 mm and span = 2200 mm. For the cut-out, a rectangular shape with constant width of 200 mm has been used, while the length parallel to the supporting line was varied considering three values; 200, 400, and 600 mm. All slabs were reinforced with a single bottom steel mesh with a longitudinal reinforcement ratio of 0.65%. The slabs having cut-outs were divided into three groups (I, II and III); each one included three different cut-outs. The slabs of group I were tested without strengthening. On the other hand, group II was strengthened at the tension side only, whereas, group III was strengthened at both tension and compression sides. Based on the experimental findings, the load-carrying capacities of group II raised by 15–57% compared to group I; however, this increase was accompanied by a significant decrease in the developed ductility where the displacement-based ductility index could be dropped by 58% for the slab having cut-out length of 600 mm. For group III, the application of SHCC plates at both tension and compression sides enabled the strengthened slabs to restore nearly the lost capacity resulting from providing the cut-out with a good ductility performance.

1. Introduction

Often, the functional requirements entail introducing cut-outs (post-construction openings) in existing Reinforced Concrete (RC) slabs for facility requirements; installation of elevators, escalators, or utilities such as heating, air conditioning, sewage pipes, or wiring ducts. Creating a cut-out leads to a break in the continuity of the slabs' loading trajectories [1–4], which reduces the load-carrying capacities and stiffness of the slabs. Thus, great attention has to be paid to an appropriate strengthening approach to restore the flexural strength of slabs including cut-outs.

Numerous retrofitting/strengthening techniques have been developed to restore/upgrade the strength of assigned RC slabs. These techniques include; section enlargement, concrete patching and external plate bonding using either steel plates or Fiber-Reinforced Polymer (FRP) plates/sheets. Strengthening RC slabs by adding a new layer of concrete is one of the common strengthening strategies [5]. However, adjoining a fresh concrete layer to an older concrete member may produce durability problems such as de-lamination or cracking along the contact surface between the two materials. This is attributed to the differential movement between the substrate concrete and the new overlay caused by temperature variations, shrinkage, or both [6,7]. Thus, good surface preparation and/or using proper shear connectors between the two layers is an important issue [8]. Another strengthening method is Externally Bonded (EB) steel plates. In this technique, the steel plates can be accomplished using either bolting or adhesive bonding. Previous research work proved the effectiveness of the EB steel plates to increase the flexural capacity as well as reduce crack width and

* Corresponding author at: Structural Engineering Dept., Faculty of Engineering, Tanta University, Tanta 31511, Egypt.
E-mail address: ali_hassan@f-eng.tanta.edu.eg (A. Hassan).

https://doi.org/10.1016/j.engstruct.2022.114149
Received 29 August 2021; Received in revised form 26 February 2022; Accepted 13 March 2022
Available online 19 March 2022
0141-0296/© 2022 Elsevier Ltd. All rights reserved.

deformations at all load levels [9–11]. However, external steel plates are susceptible to corrosion damage that requires an additional cost for protection. In addition, if mechanical anchorage is used instead of the epoxy adhesive, stress concentration at the anchorage zone is produced [11].

FRP materials have numerous advantages such as high strength, lightweight and non-corrosive material. Employing these advantages, there is a wide range of recent applications of these materials. The Externally Bonded (EB) technique was applied due to its simple installation procedure. The flexural response of RC slabs with cut-outs strengthened with EB-CFRP sheets has been reported by several researchers [12–14]. As per [12–14] observations, the FRP-strengthened slabs achieved higher load-carrying capacities when compared with their un-strengthened counterparts. However, most of the FRP-strengthened slabs failed by debonding of the FRP from the concrete substrate. The debonding was reported to initiate at cracks that propagated from the cut-out corners due to stress concentrations. This debonding mode is well known as Intermediate Crack (IC) induced interfacial debonding or simply IC debonding [12–14]. The Near Surface Mounted (NSM) technique has been adopted to avoid debonding failure. The NSM technique involves embedding strengthening bars or strips and filling material into precut grooves that are oriented along the concrete cover. The NSM technique has less exposure to the hostile environment. In addition, the NSM technique has a good bond efficiency than the EB technique because the former has a higher contact area with the substrate concrete than the latter. Therefore, the EB technique is more prone to debonding failures than NSM FRP strips [15]. Thus, compared to the EB technique, the NSM technique showed a higher anchoring capacity to the FRP material. In consequence, high tensile stress could be mobilized in the FRP strengthening material, thus, the load-carrying capacity of a strengthened member is not limited by the premature debonding failure mode [16,17]. However, some drawbacks of FRP materials still exist, such as, FRPs have low fire resistance and this requires expensive fire protection cost [18].

Strain Hardening Cementitious Composites (SHCC) is a new class of high-performance fiber-reinforced cementitious mortars. The outstanding material characteristics of the SHCC are acquired by deliberately tailoring three phases: fiber, matrix, and fiber/matrix interface, based on micromechanics theory [19–22]. Under tensile stresses, SHCC features a high strain capacity of more than 3%, which represents around a hundred times the maximum tensile strain value of Ordinary Concrete (OC) [23]. Moreover, instead of one single localized fracture crack in OC under tension, SHCC exhibits multiple micro-cracks with crack width below 100 μm [24,25]. Such tiny cracks in SHCC can improve the damage pattern of SHCC-concrete composite members [26–28]. In addition, for further increase in the tensile strain capacity of SHCC material, several researchers recommended the use of embedded steel reinforcement inside the SHCC members [29,30]. Fischer and Li [31] reported the improvement in tension stiffening behaviour of elements composed of SHCC and steel reinforcement. Also, Rokugo et al. [32] reported the enhancement due to steel reinforcement on the structural performance of steel/SHCC composite elements. Kunieda et al. [33] revealed the effectiveness of steel reinforcement in improving the post-cracking stiffness and post-ultimate ductility of specimens subjected to direct tension.

Considering the abovementioned exclusive characteristics, SHCC has been successfully used in the practical infrastructures to improve their strength, resilience and serviceability, such as coupling beams in high-rise buildings, seismic dampers in bridge and dam repair, etc. [34,35]. In laboratory tests, the performance of SHCC strengthened elements has been evaluated through various experiments which revealed the enhanced structural performance with the use of SHCC material

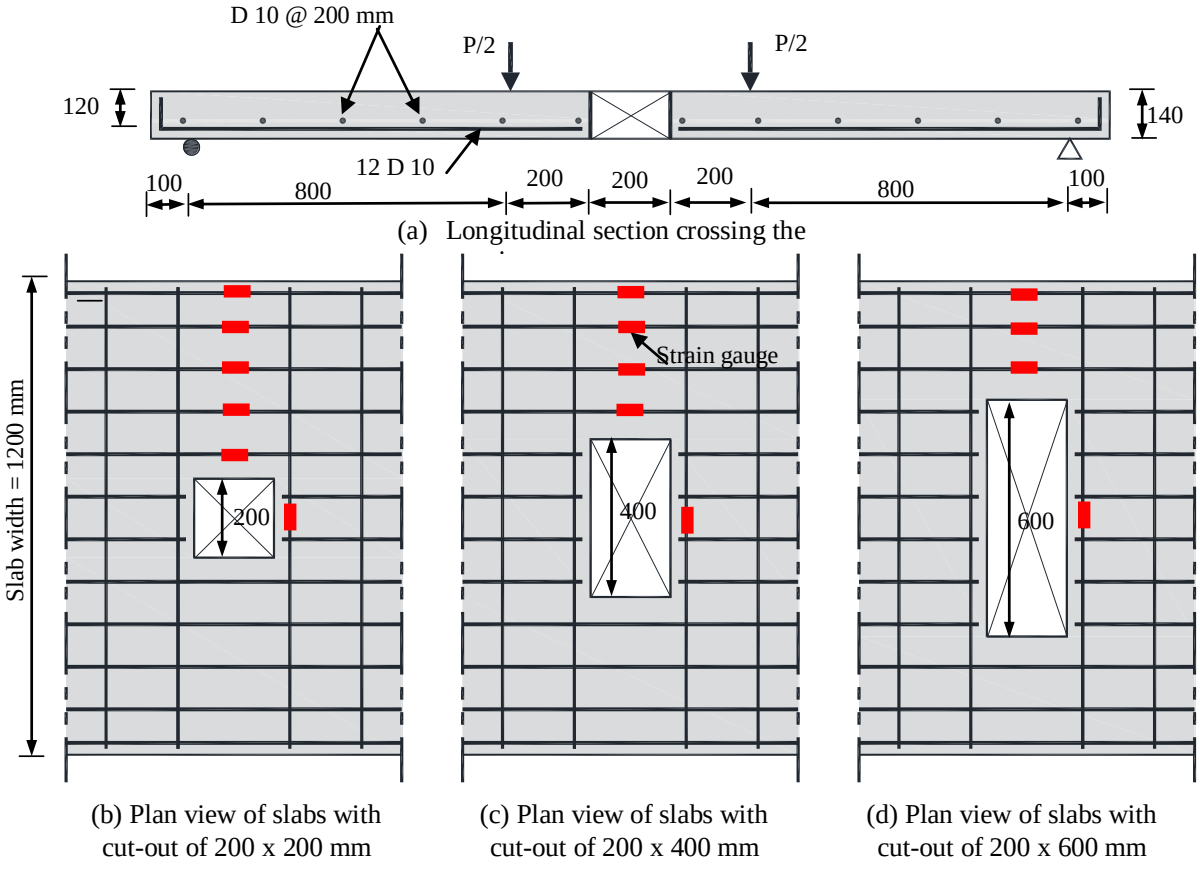


Fig. 1. Reinforcement details of the tested slabs (All dimensions in mm).

[36–41]. Despite the numerous advantages of SHCC, this material shows higher shrinkage and volumetric changes [42]. For ordinary concrete, the ultimate drying shrinkage strain with a magnitude of about 400–600 μm/m will be produced under traditional drying conditions of 20 °C and 60% relative humidity [43]. Whereas, the ultimate drying shrinkage strain of the conventional SHCC is about 1200–1800 μm/m under the same drying conditions [44,45]. Compared to traditional concrete, the high shrinkage strain of SHCC is attributed to the high quantity of cement used in the SHCC mix. Therefore, shrinkage-induced cracking may happen with the application of the fresh SHCC material to an existing concrete member. Thus, this composite material needs a special treatment, otherwise, durability problems may appear.

To preclude the issues of volumetric changes associated with SHCC material, precast and cured SHCC plates have been proposed for strengthening applications. Afefy et al. [46] examined the structural performance of RC simply supported slabs provided with precast SHCC plates. Precast SHCC strips were placed in the tension side of one-way RC slabs below the main tension steel reinforcement. The SHCC strips enhanced the flexural performance of the strengthened slabs at both service and ultimate Limit States. Hassan et al. [47] used precast thin SHCC plates to restore the shear capacity of RC beams with web opening. The strengthened beams demonstrated a distinguished performance in terms of ultimate capacity and ductility. Afefy et al. [48] evaluated the strengthening of shear-critical RC beams using NSM precast SHCC plates. The experimental test results showed that the use of precast SHCC significantly increased the ultimate shear capacity and ductility of the strengthened beams.

In most of the previous research work, when cut-outs in RC slabs are made, the common practice is to compensate the cut reinforcement by another strengthening material at the slab's tension side only [1–5,12,13]. However, the cut-out includes both reinforcing steel as well as concrete. For a decreased concrete section due to a cut-out, the compensation of tension steel increases the forces acting on concrete at the compression side that may lead to a compression failure for highly reinforced sections. In addition, the compensation of tension steel shifts the neutral axis of the RC section resulting in a decrease in the lever arm of the resisting moment. Consequently, the original strength cannot be restored, in addition, a great loss in the ductility is expected. In the current research, using precast reinforced SHCC plates, two types of strengthening procedures were employed and evaluated. The first strengthening procedure compensates the cut of reinforcement with equivalent precast SHCC plates bonded to the tension side of the slabs with cut-outs. At the second strengthening procedure, another set of slabs with cut-outs (similar to those of the first procedure) was strengthened at both tension and compression sides using the SHCC plates. The SHCC material was applied to the slabs in the form of precast plates to avoid the drawbacks of volumetric changes associated with SHCC material. In addition, the NSM technique was used in the current research to obtain a better bond performance between the strengthening material and the substrate concrete. As previously recommended, during the fabrication process, all plates were internally reinforced with steel bars to increase their strength and ductility. The test results in the forms of ultimate loads, mode of failure, load-deflection behaviour and crack width results for the tested slabs were presented and discussed. A flexural strength prediction model was verified with the experimental results. Furthermore, the accuracy of the crack width prediction model of Eurocode2 was evaluated.

2. Experimental work program

2.1. Test specimens

The current experimental work program consisted of nine RC one-way spanning slabs with cut-outs in addition to a reference slab without cut-out. As shown in Fig. 1, all slabs had similar dimensions and internal reinforcement steel. Each slab had 1200 mm width, 140 mm thickness, 120 mm effective depth, and a total length of 2400 mm, while the effective span was 2200 mm. In this investigation, three different cut-out sizes of 200 × 200, 200 × 400, and 200 × 600 mm were tested. All cut-outs were situated in the zone of the maximum moment and the length of the cut-out was parallel to the slab's transverse direction. All slabs were reinforced with a single mesh of high-strength deformed steel bars (type B420DWR, as per ECP-203 code [49]). The used mesh consisted of 12 D 10-mm in the longitudinal direction and 12 D 10-mm as distributed steel in the other direction. The used flexural reinforcement ratio was 0.65% and it was designed to ensure a tension failure mode as per the current ACI 318-19 code [50]. To simulate a cut-out sawn into a constructed slab, as shown in Fig. 2, no additional reinforcement was provided around the cut-outs' edges.



Fig. 2. Image of a test slab after placing of the steel reinforcement cage.

2.2. Test parameters

The nine RC slabs with cut-outs were divided into three groups. Each group included three slabs with three different cut-out lengths (L_o) of 200, 400 and 600 mm. The slabs of group I were tested without strengthening, whereas, the other groups were strengthened with two different strengthening procedures. The details of the strengthened slabs of groups II and III are shown in Fig. 3. For group II, each slab was strengthened in tension side only using two precast NSM-SHCC plates (plate at either side of the cut-out). The used plates had a thickness of 20 mm to be easily accommodated in the concrete cover. Previous research work reported a great enhancement in the post-cracking behaviour of steel reinforced SHCC members subjected to tensile forces [29–33]. Thus, during the fabrication of the SHCC plates, each of them was internally reinforced with mild steel bars with an 8 mm diameter (the plate's reinforcement ratio was 7.5%). The plate's cross-sectional area was designed to be equivalent to the loss of the internal bars upon creation of the cut-outs taking into account the relevant material properties (i.e. the tensile capacity provided by the reinforced SHCC plates is almost equal to the steel bars that were cut). Thus, NSM-SHCC plates with widths of 100, 200 and 300 mm were used with slabs having cut-outs' lengths of 200, 400 and 600 mm, respectively. The length of the SHCC plates was designed to avoid debonding failure based on the mechanical properties of the used bonding epoxy. The used development length was 550 mm length, as shown in Fig. 3. For group III, the idea was to add SHCC plates also in the compression site to compensate the added SHCC plates in the tension side, which lead to higher compression forces, for which the concrete was not prepared/designed. Thus, the slabs were symmetrically strengthened in both tension and compression sides using NSM-SHCC plates. The used plates have the same geometrical dimensions and reinforcement as those used in group II.

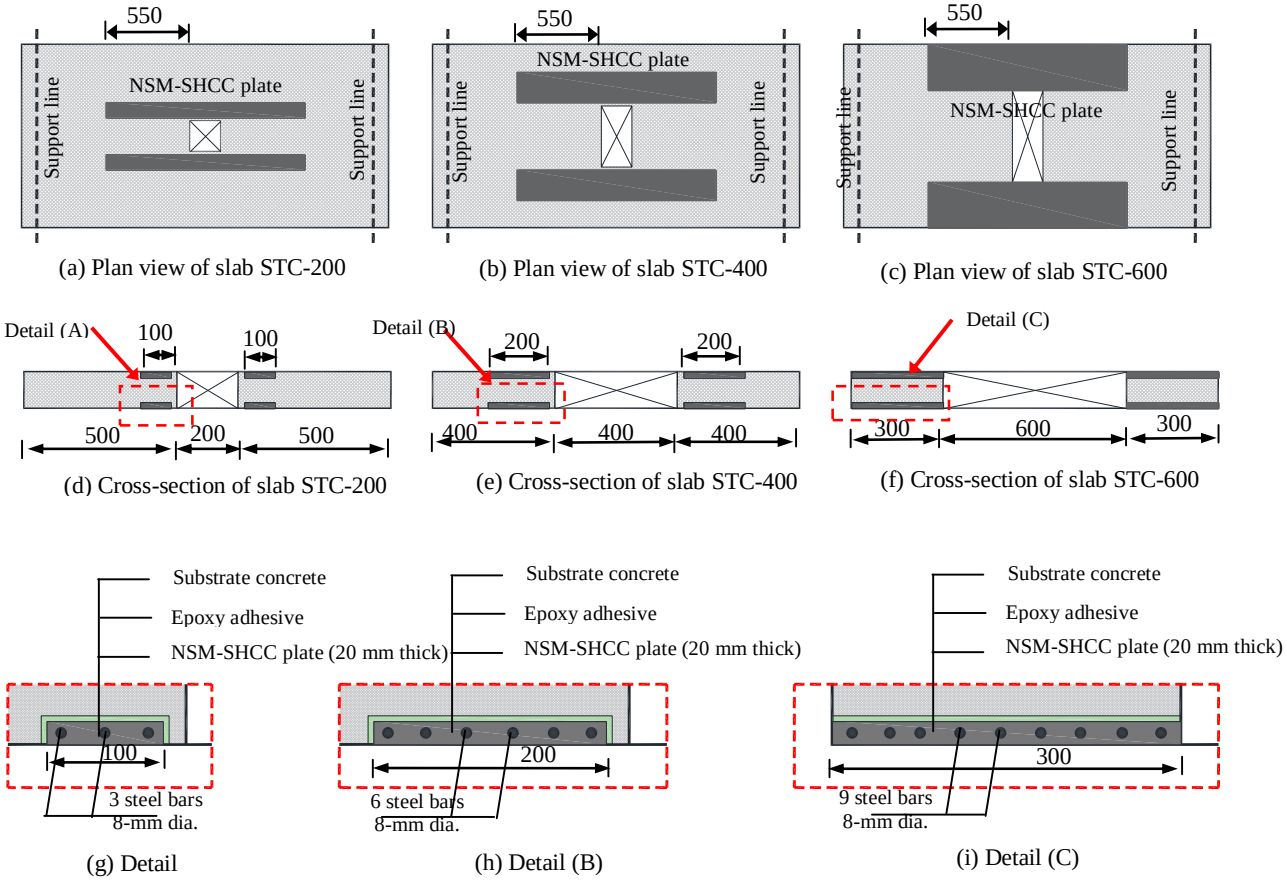


Fig. 3. Details of the slabs strengthened using NSM-SHCC plates (All dimensions in mm).

Table 1
Description of test specimens.

Group	Slab's designation	Cut-out size		Strengthening regime
		width, mm	length, mm	
Control	SC	without cut-out		Without strengthening
Group I	S-200	200	200	Without strengthening
	S-400	200	400	
	S-600	200	600	
Group II	ST-200	200	200	Strengthened with NSM-SHCC plates at tension side only
	ST-400	200	400	
	ST-600	200	600	
Group III	STC-200	200	200	Strengthened with NSM-SHCC plates in both of tension and compression sides
	STC-400	200	400	
	STC-600	200	600	

2.3. Designation of the slabs

As shown in Table 1, the control slab without a cut-out was designated by the capital letters SC. on the other hand, the slabs of group I were symbolized by the letter S followed by the cut-out length. For example, the designation S-200 refers to the unstrengthened slab with a cut-out length of 200 mm. The strengthened slabs of group II were designated by ST followed by the cut-out length. Finally, the slabs of group III were designated by STC followed by the cut-out length.

2.4. Material properties

A ready mix concrete patch was used in the fabrication of the tested slabs. As listed in Table 2, the mix ingredients consisted of ordinary Portland cement (type-I), sand, crushed limestone with a maximum aggregate size of 10 mm, and water. At the test date, compressive and indirect tensile tests were performed on three standard cylinders of size 150 × 300 mm. Fig. 4 shows the uniaxial compressive stress-strain curve of the used concrete. For clarity, the results of one specimen are presented, as the tested specimens showed almost similar stress-strain curves. As shown in Fig. 4, the average compressive strength of three standard cylinders was 24.9 MPa. On the other hand, the average splitting tensile strength of three standard cylinders was 2.91 MPa.

All plates were cast at the same time using the same SHCC mixture to ensure similar properties. The mixture proportions are listed in Table 2. The SHCC ingredients were; ordinary Portland cement (type I), silica fume, fine aggregate, water, fibers (polypropylene fibers), and water-reducing admixture. The SHCC mixture had a water-to-binder material ratio (W/B) of 0.20 and a silica fume to cement ratio of 0.18, by weight. To obtain multiple micro-cracking and strain hardening behaviour, it is

Table 2
Mix proportions of the used SHCC and concrete for cubic meter (kg/m^3).

Material	Cement	Sand	Coarse aggregate	Silica fume	Fibers (volumetric ratio)	Super plasticizers	Water	Water-to-binder ratio
SHCC	1342	157.9	–	237	16.20 (2.0%)	31.6	312.1	0.20
Concrete	350	530	1300	–	–	–	175	0.5

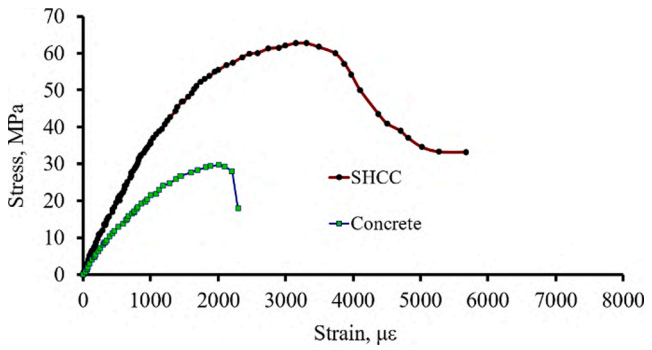
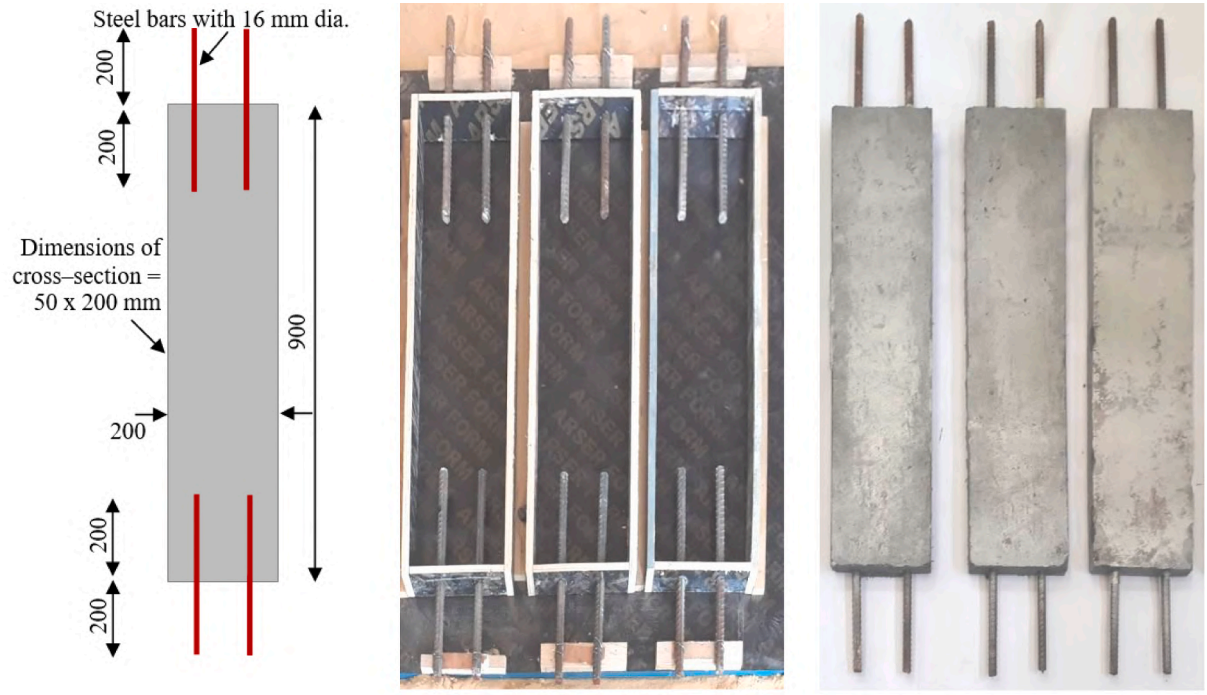


Fig. 4. Samples of the stress-strain curves of SHCC and concrete under uniaxial compressive test.

necessary to minimize the fracture toughness of the matrix [51]. Thus, only fine aggregates are recommended to be used for the production of SHCC; silica sand with a normal maximum size of 1.0 mm was used for the production of SHCC mixture. High-strength polypropylene (PP) fibers with a volume fraction of 2% were used. As included in the manufacturer's datasheet, the diameter and length of the fibers were 25 μm and 12 mm, respectively.

The uniaxial compressive strength of the used SHCC was determined by testing three cylinders having a size of 50 × 100 mm, as per JSCE recommendations [52]. A sample of the obtained compressive stress-strain curves of the SHCC material is depicted in Fig. 4. As shown in Fig. 4, the average compressive strength of the SHCC material was 60.8 MPa. On the other hand, the tensile strength of the used SHCC was determined by testing three specimens. The dimensions of the test specimens were chosen based on Kunieda et al. recommendations [33], to avoid the size effect, they recommended carrying the uniaxial tensile



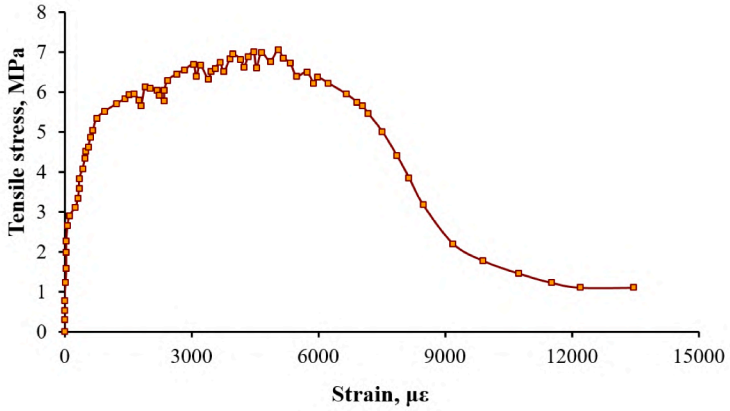
(a) Dimensions the tested specimens (dimensions in MM)

(b) the tested specimens prior to casting of SHCC

(c) the tested specimens after casting of SHCC



(d) Uniaxial tension test setup



(e) A sample of the stress-strain curves of SHCC under uniaxial tension test

Fig. 5. Details of the uniaxial tension test of SHCC material.



(a) Image of SHCC plates reinforcement

(b) Image during casting of SHCC

(c) Samples of the used Precast SHCC plates

(d) Image during creation of the required grooves

(e) Image during the application of the SHCC plates

(f) Image after the completion of the strengthening process

Fig. 6. Different stages of strengthening application.

tests on real scale specimens. The details of the recommended test specimens are shown in Fig. 5. The test specimen had a cross-section of 50 × 200 mm and a length of 900 mm. To facilitate the testing process, two high-strength steel bars of 16 mm diameter were placed at each end of the tested specimen, as shown in Fig. 5. The embedded length (200 mm) of the used bars was carefully designed to avoid any possible bond failure. Fig. 5d shows a sample of a uniaxial test specimen during the test. A sample of the obtained tensile stress-strain relationship is shown in Fig. 5e. The average first crack and the average ultimate strengths of the tensile test specimens were about 3.01 and 7.02 MPa, respectively.

The tensile properties of the used steel reinforcement bars were determined by the test of three standard specimens for each diameter. For the steel bars with 10 mm diameter (type B420DWR), the average yield and ultimate tensile strengths were 479 MPa and 634 MPa, respectively. For the steel bars with 8 mm diameter (type B220D-P), the average yield and ultimate tensile strengths were 220 MPa and 355 MPa, respectively.

A structural epoxy mortar (MasterBrace ADH 2200) was used to bond the precast plates to the substrate concrete. As per the manufacturer's specifications, the used epoxy mortar has a density of 1.85 kg/L and its final setting time is 12 h. The used epoxy reaches its complete strength after 7 days. The compressive, flexural, tensile strengths of the used epoxy are about 65, 20 and 10 MPa, respectively. Whereas, as per the manufacturer's datasheet, the ultimate bond strength for the used epoxy is more than 2.00 MPa.

2.5. Fabrication of the SHCC plates and strengthening application

As shown in Fig. 6, the SHCC plates were cast into wooden formwork. Prior to the casting of SHCC, the required reinforcement was provided to the SHCC plates. The SHCC material has a self-compacting characteristic, thus, no vibrators were used during the casting process. To obtain a similar distribution of fibers in all plates, the SHCC mix was poured from an end of the wooden forms and allowed to flow to the other end. When the wooden forms were filled with the SHCC material, the plates' surfaces were leveled and covered with a plastic sheet to prevent moisture loss. After 24 h, the plates were de-molded and then, were submerged in a water pool for 14 days.

Fig. 6a to 6e summarize the preparation and the strengthening procedure of the strengthened slabs. Grooves with 22 mm depth were created on surfaces of the slabs based on the strengthening configuration. Then, the created grooves were cleaned from dust and fine particles using an air compressor. The grooves were filled to halfway with the epoxy resin, and then the plates were placed in the groove and then lightly pressed. This forced the resin to flow around the plates in order to fill the voids between them and the sides of the grooves. Finally, the redundant resin that came out from the groves was removed, and the surfaces around the plates were leveled.

2.6. Test setup and instrumentations

Fig. 7 shows the used four-point loading test setup. A series of 100 mm linear variable displacement transducers (LVDTs) were used in order to measure the vertical deflection at mid-span point, under loading points, and over the two supports of the tested slabs. In addition, 10 mm electrical strain gauges were used to measure the developed strains in the longitudinal steel reinforcing bars. An optical microscope of 0.01 mm accuracy was used to measure the main crack width. All slabs were

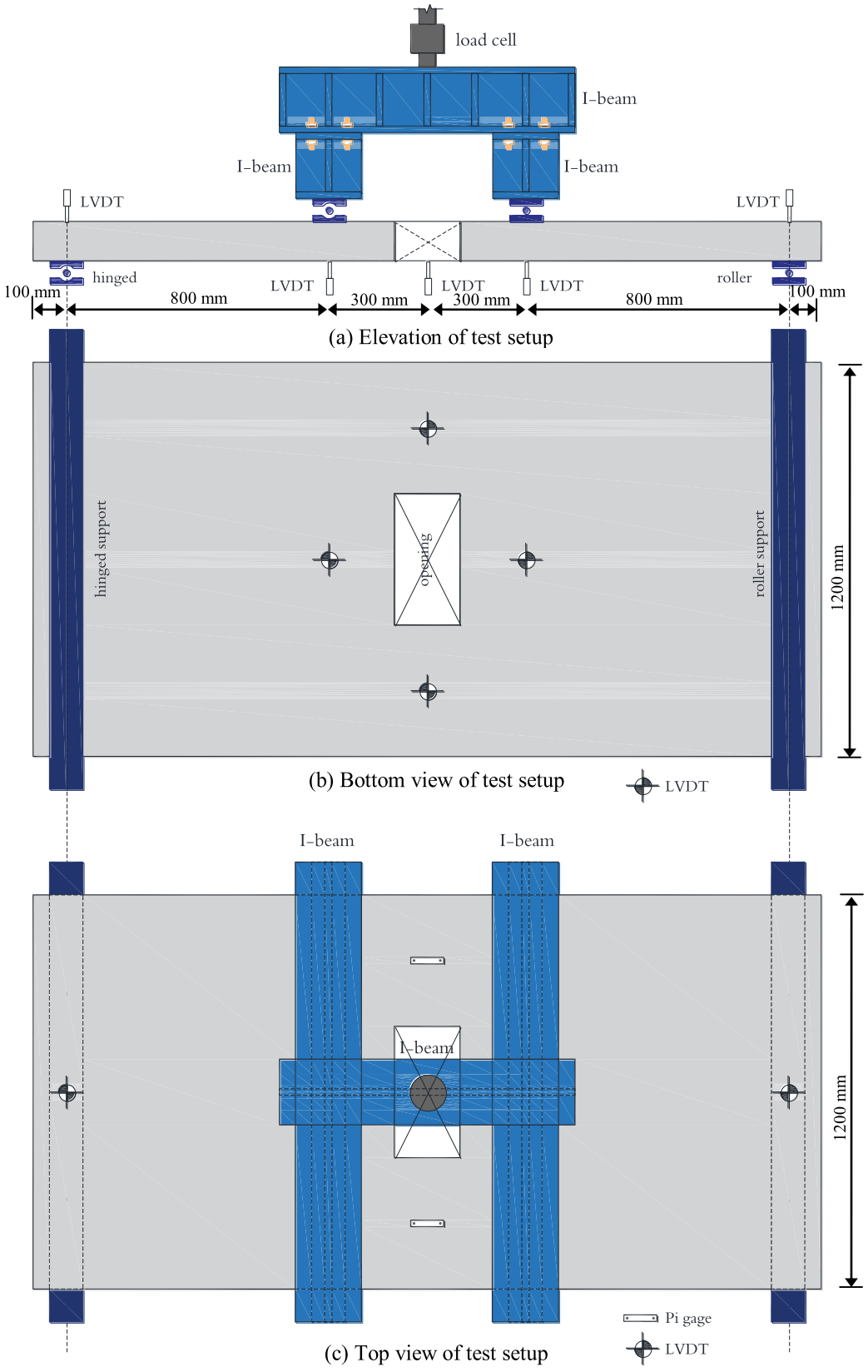


Fig. 7. Test setup and instrumentation.

loaded with two-line loads at a distance of 800 mm from the supports. The acting load was measured by a load cell of 200 kN capacity. The vertical deflections, the gauges readings as well as load readings were recorded using an automatic data logger unit.

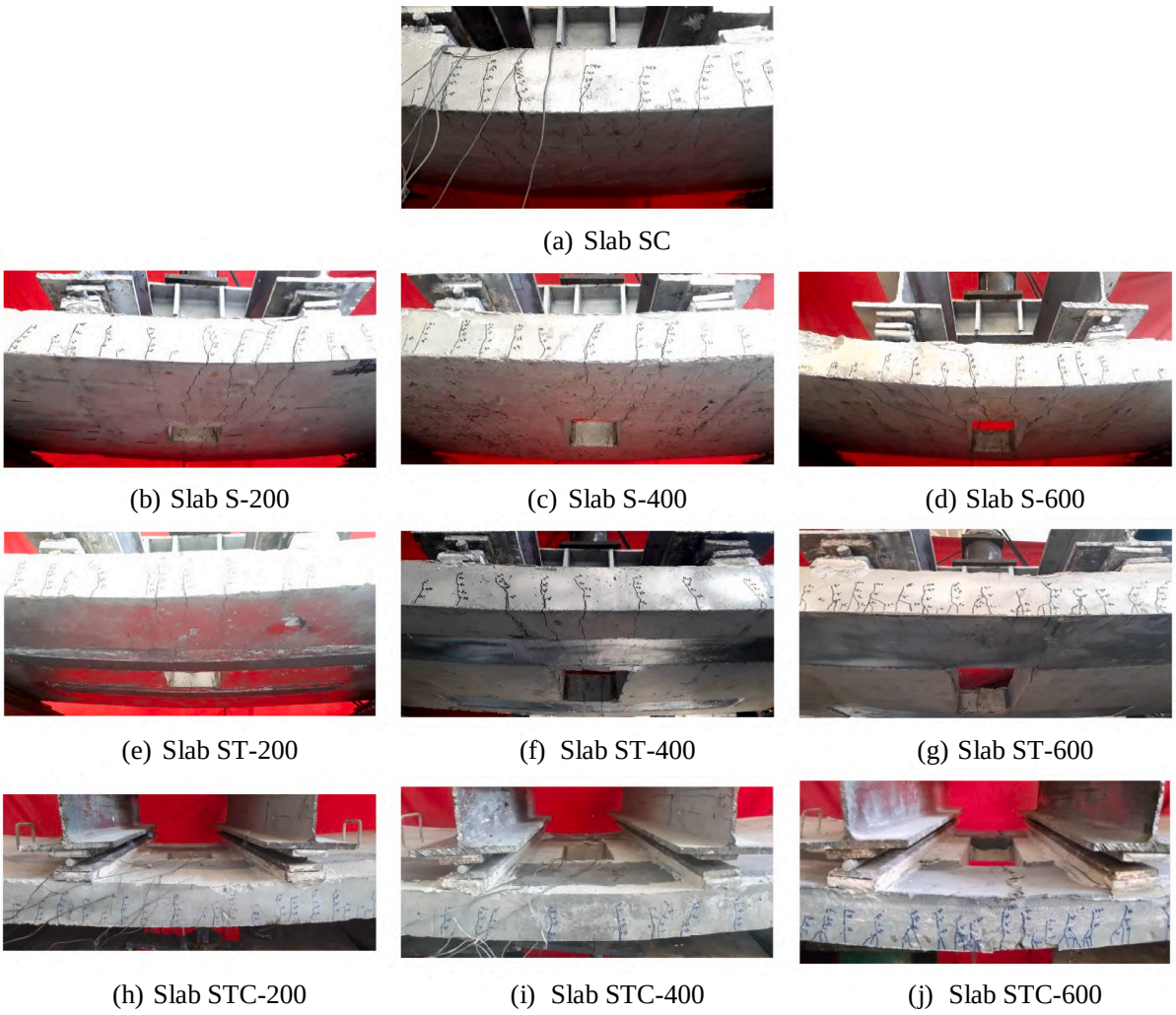


Fig. 8. Visual slab damage upon completion of testing.

3. Experimental results

3.1. Failure mode

Fig. 8 shows the mode of failure of the tested slabs at the end of the testing process. As shown in Fig. 8, the control slab, as well as the strengthened slabs exhibited flexural tension failure mode, as configured, due to the yielding of tension steel bars followed by crushing of concrete at the compression side. However, most of the FRP strengthened slabs with an opening (cut-out) demonstrated crack-induced debonding failure [12–18], the slabs strengthened with NSM-SHCC plates at the tension side demonstrated rupture of SHCC plates without any sign of detachment between the substrate concrete and the SHCC plates. Furthermore, as shown in Fig. 8h to 8j, when the SHCC plates were used at compression side (with group III), at failure, crushing of SHCC plates took place without debonding between the substrate concrete and the SHCC plates.

3.2. Crack patterns

Fig. 9 shows graphical drawings of the crack patterns in the bottom side of the tested slabs at the end of the tests. For the control slab (SC), which was cast without a cut-out, transversal flexural cracks parallel to the edge supports were noticed. These cracks were widely spread over the whole length of the slab. On the other hand, for the slabs having cut-outs, initially, diagonal cracks began to develop from the cut-out corners then extended towards the outer edges of the slab. By increasing the applied load, additional flexural cracks formed in the constant moment zone and then into the shear span zone. As the load increased, the existing cracks became wider, especially the diagonal cracks at the corners of the cut-out. Comparing the cracks' patterns of the tested slabs, it is obvious that while the cut-out length increased, the inclination of the corner cracks increased as well as the total number of the developed cracks decreased. As for the slabs strengthened with SHCC-plates, the crack patterns were as their counterparts slabs without strengthening but with an obvious increase in the number of the developed cracks. It is worth mentioning that, the SHCC plates exhibited multiple fine cracks versus localized wide cracks in the concrete substrate. As shown in Fig. 9, the density of the cracks in the SHCC plates was not equal over the plate length. The cracks density increased near the cut-out zone and then decreased gradually whenever approaching from the plate end. This is attributed to the decrease of internal tensile force in the SHCC plate by approaching its ends.

3.3. First crack load

Table 3 reports the first crack loads (P_{cr}) and the ultimate loads (P_u) for the tested slabs. The first crack load was determined based on the load-deflection response corresponding to the first change in the slab's stiffness. As presented in Table 3, slab SC (without cut-out) showed the

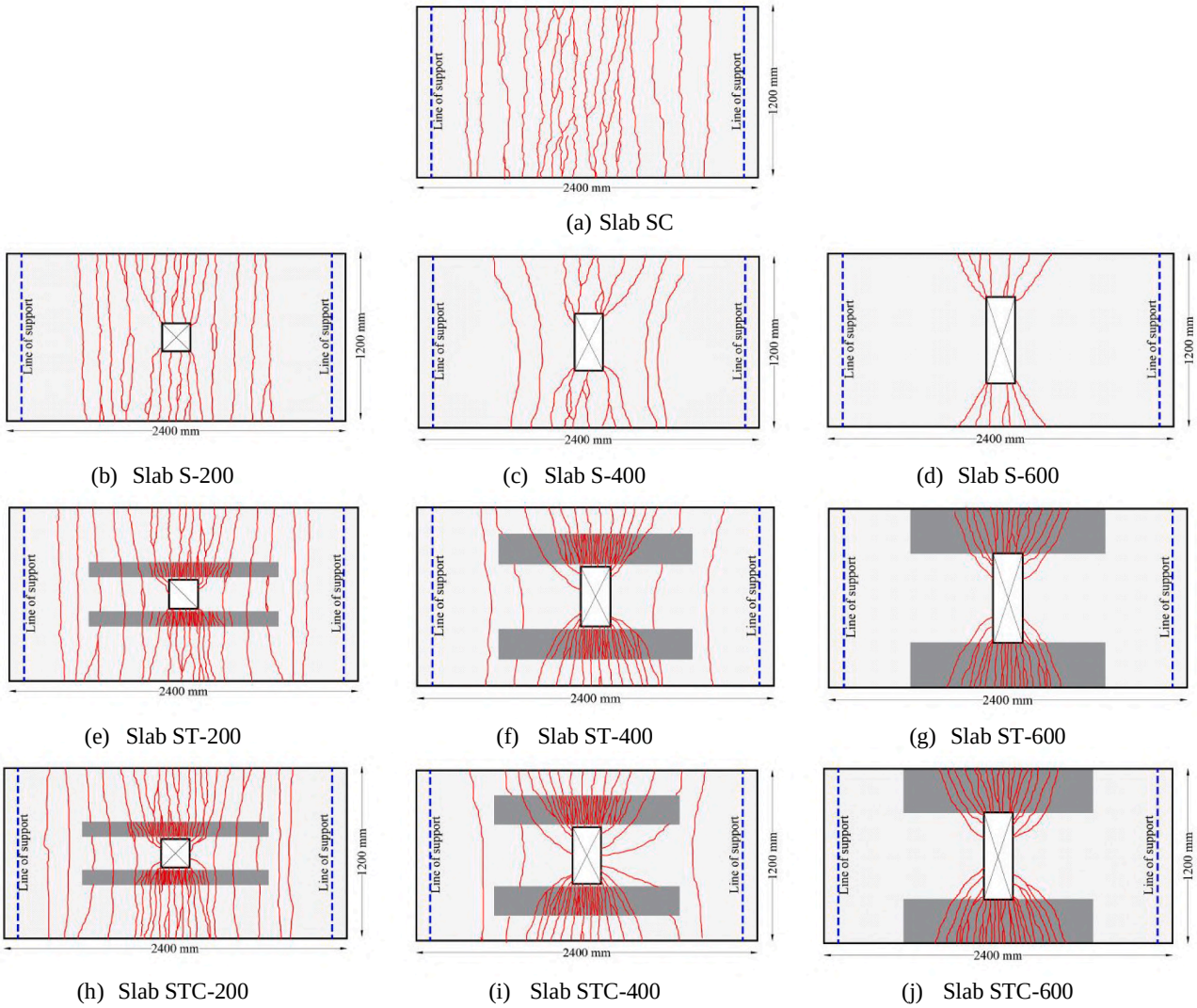


Fig. 9. Sketch of final crack pattern of the tested slabs.

Table 3
Summery of test results.

Group	Slab's designation	At first flexural crack			At yield load of internal steel reinforcement				At ultimate load			
		P_{cr}, kN	$P_{cr}/P_{cr,SC}$	Δ_{cr}, mm	P_y, kN	$P_y/P_{y,SC}$	Δ_y, mm	W_y, mm	P_u, kN	$P_u/P_{u,SC}$	Δ_u, mm	W_u, mm
Control	SC	41	1.00	2.11	127	1.00	14.57	0.31	145	1.00	51.58	1.71
Group I	S-200	34	0.83	2.90	97	0.76	14.71	0.35	120	0.83	51.69	2.20
	S-400	27	0.65	2.81	79	0.62	14.73	0.41	94	0.65	51.96	2.21
	S-600	20	0.49	3.08	56	0.44	14.75	0.50	67	0.46	52.12	2.31
Group II	ST-200	35	0.85	2.73	121	0.95	15.82	0.32	138	0.95	44.68	1.15
	ST-400	29	0.71	2.78	108	0.85	20.64	0.42	122	0.89	39.48	1.30
	ST-600	23	0.56	2.81	98	0.77	22.5	0.48	105	0.77	33.81	1.40
Group III	STC-200	35	0.85	2.70	122	0.96	15.01	0.33	145	1.00	51.75	1.28
	STC-400	30	0.73	2.75	112	0.88	17.23	0.42	133	0.92	51.51	1.30
	STC-600	24	0.58	2.86	104	0.82	19.03	0.46	124	0.86	50.18	1.29

P_{cr} = first crack load; P_y = yield load; P_{ult} = ultimate load; Δ_{cr} = deflection at cracking load; Δ_y = deflection at yield load; Δ_{ult} = deflection corresponding to ultimate load; W_y = major flexural crack width at yield load; W_u = major flexural crack width at ultimate load.

highest cracking load of 41 kN. This value represents 28% of its ultimate load. On the other hand, the cut-outs showed a dramatic decrease in the first crack load. The lowest cracking load due to the effect of the cut-out was achieved by slab S-600. The first crack took place at a load of 20 kN, which represents 49% of that achieved by the control slab (without cut-out). As for the strengthened slabs, the application of the SHCC plates at the tension side showed a slight improvement in the first cracking capacity of the slabs. The first crack loads of slabs ST-200, ST-400 and ST-600 were 35, 29 and 23 kN, respectively, these values represent 3, 7 and 15% higher than those achieved by slabs S-200, S-400 and S-600, respectively. This enhancement is attributed to the addition of the SHCC plates, which delayed the first crack initiation. As expected, the slabs of group III (strengthened at both tension and compression sides) showed insignificant improvement in the first crack load, compared with ST

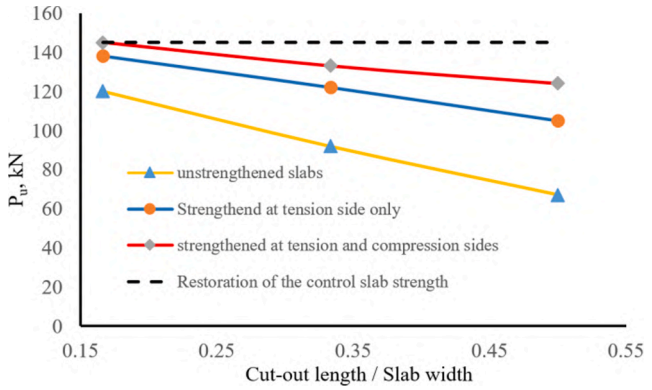


Fig. 10. Relation between the ultimate capacity and cut-out length/slab width ratio.

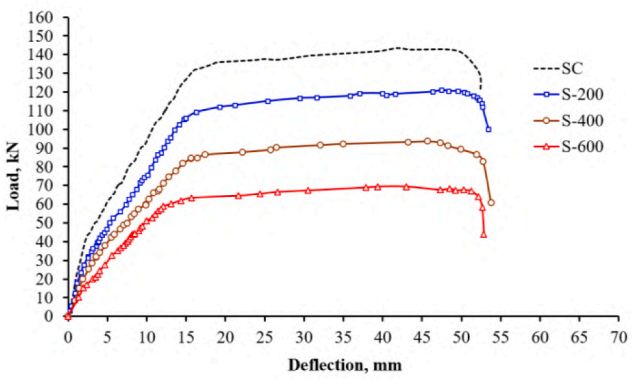
specimens. The highest improvement in first crack load was obtained by slab STC-600 (24 kN), which represents about 4% higher than that achieved by slab ST-600 (23 kN).

3.4. Ultimate loads

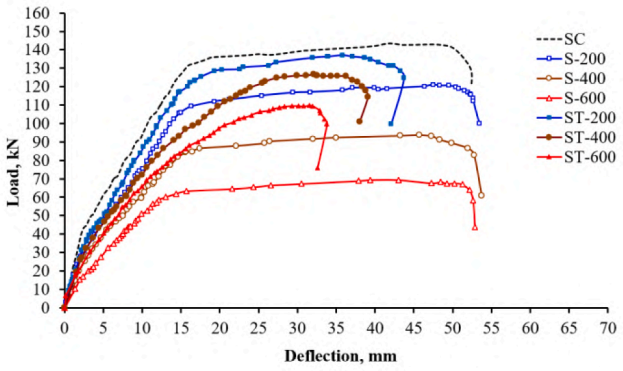
Column 8 of Table 3 summarizes the ultimate loads (P_u) for the tested slabs. In addition, Fig. 10 shows a relation between the ultimate loads versus the cut-out length/slab width ratio. As shown in Fig. 10, the unstrengthened slabs with cut-out achieved lower capacities than those of the control and the strengthened slabs. The achieved capacity was inversely proportional to the cut-out length. The achieved loads of slabs S-200, S-400 and S-600, respectively, were 83, 65 and 46% of that of slab SC (145 kN). As for group II, however, the cut reinforcement was replaced by precast SHCC plates at the tension side, the strengthened slabs did not achieve the ultimate load of the control slab. The achieved loads of slabs ST-200, ST-400 and ST-600, respectively, were 95, 84 and 72% of that of slab SC. The test results confirm the results obtained by Afefy and Fawzy [1], Smith and Kim [4] and Florut et al. [13]. For slabs with cut-outs, the addition of strengthening material at the tension side only led to an increase in the compressive force in concrete and a decrease in the lever arm of the resisting moment of the concrete section [1,4,10]. Thus, the flexural capacity of the strengthened slabs with cut-outs increased but did not reach the capacity of the control slab (SC). To highlight the importance of adding a strengthening material at both tension and compression sides of slabs with cut-outs, the slabs of group III were tested. Slabs STC-200, STC-400, and STC-600 showed increases of about 6%, 9% and 18%, respectively, above their alternatives ST-200, ST-400, and ST-600. This enhancement is attributed to the use of high strength material (SHCC) at the compression side that decreased the depth of the compression zone, and then increased the lever arm of the resisting moment of the concrete section. On the other hand, the obtained values for slabs STC-200, STC-400, and STC-600, respectively, represent 100, 92 and 86% of that achieved by the control slab SC. The increase in the cut-out size increases the stress around the opening this decreased the ultimate strength.

3.5. Load-deflection response

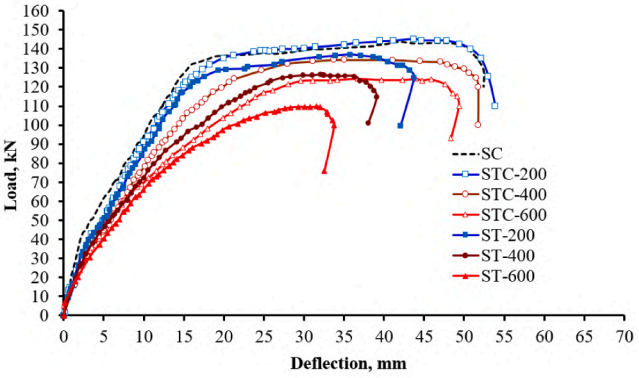
The load-deflection (mid-span deflection) curves for the tested slabs are shown in Fig. 11. As mentioned before in section 2.6 the mid-span deflection was recorded at the two sides of the cut-out. As expected, the values of mid-span deflection at the two sides of the cut-out were found to be virtually identical due to the symmetrical loading scheme. In addition, the LVDT's which were positioned at each support recorded minimal movements. Generally, as shown in Fig. 11, each slab showed a linear behaviour up to the first crack load. Beyond that, a significant change in the slope of the load-deflection curve was noticed. Increasing



(a) Curves of slab SC and group I.



(b) Curves of slab SC, group I and group II.



(c) Curves of slab SC, group II and group III.

Fig. 11. Load deflection curves of the tested slabs.

the applied load, the yielding of the steel reinforcement took place, and then a plateau in the load-deflection curve was observed till the complete failure.

For the unstrengthened slabs of group I, as shown in Fig. 11a, the increase in cut-out length showed to decrease in the slab's stiffness corresponding to an increase in the deflection at all loading stages. At ultimate, the recorded deflections of slabs S-200, S-400 and S-600 were 51.69, 51.96 and 52.12 mm, respectively. As for the strengthened slabs of group II (strengthened at tension side only with SHCC plates), the addition of the SHCC plates increased the slab's tension stiffness. Thus, as shown in Fig. 11b, compared to the unstrengthened slabs of group I, all slabs of group II showed a good enhancement in the post cracking stiffness leading to a significant decrease in the developed deflection at

Table 4
Ductility indices for the tested slabs.

Group	Slab's designation	Displacement-based ductility				Energy-based ductility			
		Δ_y, mm	Δ_u, mm	μ_D	WRT SC	E_y, kN.mm	E_u, kN.mm	μ_E	WRT SC
Control	SC	14.57	51.58	3.54	1.00	1150	6003	5.22	1.00
Group I	S-200	14.71	51.69	3.51	0.99	960	4998	5.21	1.00
	S-400	14.73	51.96	3.52	0.99	779	4050	5.20	0.99
	S-600	14.75	52.12	3.53	0.99	617	3180	5.15	0.98
Group II	ST-200	15.82	44.68	2.82	0.80	1050	4490	4.27	0.82
	ST-400	20.64	39.48	1.91	0.54	954	3240	3.39	0.65
	ST-600	22.5	33.81	1.50	0.42	890	2505	2.81	0.54
Group III	STC-200	15.01	51.75	3.44	0.97	1170	6016	5.14	0.98
	STC-400	17.23	51.51	3.00	0.85	1156	5619	4.86	0.93
	STC-600	18.53	50.18	2.71	0.77	1120	4970	4.44	0.85

Δ_y = deflection at yield load; Δ_{ult} = deflection corresponding to ultimate load; E_y = Absorbed energy before yielding load; E_u = Absorbed energy before ultimate load; μ_D = Displacement-based ductility, μ_E = Energy-based ductility, WRT SC = with respect to control slab SC.

the same loading level. Unfortunately, the addition of tension reinforcement due to the application of the SHCC plates resulted in a reduction of mid-span deflection at ultimate load leading to a significant loss in the ductility. At ultimate, the recorded deflection values of slabs ST-200, ST-400 and ST-600, respectively, were 44.68, 39.48 and 33.81 mm, which represent 86, 76 and 65% of those of slabs S-200, S-400 and S-600, respectively. Where, these values represent 100, 99 and 97% of that achieved by the control slabs. This reflects the ability of SHCC material to enhance the ductility of the slabs when provided at the compression zone.

As for the slabs of group III which were strengthened at both tension and compression sides using precast SHCC plates, the hybrid strengthening technique showed a good restoration of ultimate capacity with enhanced ductility, as shown in Fig. 11C. This may be explained as follows; when the SHCC material was added to the slab's compression side, its high strain capacity enabled the slabs to sustain a large deformation before the occurrence of the crushing. At ultimate, the recorded deflections of slabs STC-200, STC-400 and STC-600, respectively, were 51.75, 51.51 and 50.18 mm, which represent 16, 30 and 48% higher than those of slabs ST-200, ST-400 and ST-600, respectively.

3.6. Ductility measurements

Ductility is defined as the ability of a member to perform inelastic deformations after the initial yield deformation without a decrease in the load resistance [52]. Ductility has been evaluated by a ratio named the ductility index (l). Usually, the ductility index is expressed as a ratio of curvature (u), rotation (h), absorbed energy (E), and deflection (D), at failure divided by the corresponding property at the yielding point of internal steel reinforcement. In this research, the ductility was evaluated based on both displacement and absorbed energy.

3.6.1. Displacement-based ductility

The displacement-based ductility index is obtained by Eq. (1) [53]:

$$\mu = \Delta_u/\Delta_y \quad (1)$$

where (Δ_u) is the mid-span deflection corresponding to ultimate load and (Δ_y) is the mid-span deflection corresponding to the yield load of the internal steel reinforcement.

Table 4 shows the experimental outputs pertaining to the displacement-based ductility indices for the tested slabs. As presented in Table 4, the un-strengthened slabs of group I (with cut-out) gave quite similar ductility indices compared to that of slab SC (without cut-out). For slabs SC, S-200, S-400 and S-600, the obtained values were 3.54, 3.51, 3.52 and 3.53, respectively. As for group II, the addition of NSM-SHCC plates at the tension side of the slabs showed a decrease in ductility. Moreover, the loss in ductility index rises as long as the cut-out length increases. As a consequence, the lowest value of ductility index was obtained by slab ST-600 (1.50), which represents 42% of that obtained by slab S-600 (with cut-out). This means that the increase in the ultimate capacity of the slabs of group II came at the expense of the developed ductility. As for the slabs of group III, the addition of NSM-SHCC plates at both tension and compression sides of the slabs showed to preserve the ductility of the slabs. For instance, the ductility index of slab STC-600 was 2.71, 81% higher than that obtained by slab ST-600 (1.50).

3.6.2. Energy-based ductility

The ductility can be also evaluated based on the absorbed energy. The energy-based ductility index is obtained by Eq. (2) [53]:

$$\mu_E = E_u/E_y \quad (2)$$

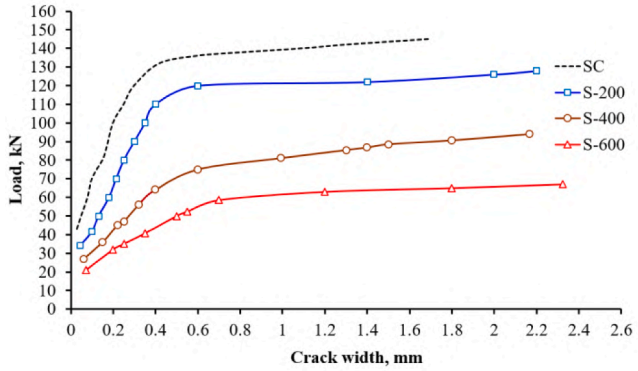
where (E_u) is the absorbed energy at ultimate load and (Δ_y) is the absorbed energy corresponding to the yield load of the internal steel reinforcement.

The elastic energy at the yield load of the internal steel (E_y), ultimate energy at the failure load (E_u), and the energy-based ductility index (μ_E) for all slabs are given in Table 4. As presented in Table 4, the energy-based ductility index showed approximately a similar trend as the displacement-based ductility index. The addition of NSM-SHCC plates at the tension side of the slabs with cut-outs showed an increase in the ultimate load and a decrease in the manifested ductility. The obtained energy-based ductility indices for slabs ST-200, ST-400 and ST-600 were 82, 65 and 55% of those obtained by slabs S-200, S-400 and S-600, respectively. On the other hand, the test results assure that the strengthening technique using upper and lower NSM-SHCC plates is favorable to compensate the reduced capacity and ductility. For slabs STC-200, STC-400 and STC-600, the obtained energy-based ductility indices were 99, 93 and 86% of those obtained by slabs S-200, S-400 and S-600, respectively.

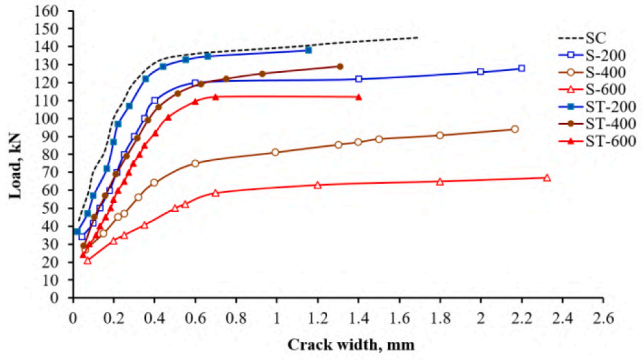
3.7. Crack width measurements

3.7.1. Load-crack width relationship

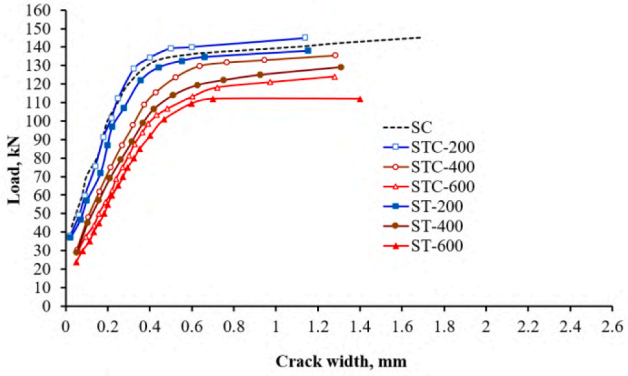
The crack width has a significant influence on the durability and appearance of RC structures. Thus, the design codes set a limiting value for allowable maximum crack width. For ordinary exposed RC buildings, both CEB-FIP [54] and ECP 203 [49] codes set a limiting value of 0.3 mm for the maximum crack width at service load level. While Eurocode2 [55] sets a limiting value of 0.4 mm. As mentioned in section 2.6, the crack width was measured using an optical microscope (0.01 mm accuracy). For the slabs with cut-outs, the maximum crack width was measured at the soffit of the slab beside the opening corner. The load versus crack width curves for all slabs are shown in Fig. 12. In addition, the test loads corresponding to crack widths of 0.1, 0.2, 0.3 and 0.4 mm for the tested slabs are summarized in Table 5. Comparing the load-crack width results for the slabs of group I shows that, increasing the cut-out length led to a dramatic increase in the crack width at all loading



(a) Curves of slab SC and group I.



(b) Curves of slab SC, group I and group II.



(c) Curves of slab SC, group II and group III.

Fig. 12. Load crack width curves of the tested slabs.

stages. At the same crack width, the load carried by slabs S-200, S-400 and S-600, respectively, ranged between 60–83%, 42–48% and 30–34% of that carried by the control slab (SC).

Increasing the reinforcement ratio of RC flexural member decreases the developed bar strain at the same load level and that decreases the developed crack width [1]. As shown in Fig. 12, all slabs of group II (strengthened with NSM-Plates) showed a lower crack width compared to group I. At crack width of 0.3 mm, the loads carried by slabs ST-200, ST-400 and ST-600, respectively, were 107, 89 and 75 kN, which represent 19, 59 and 97% higher than those obtained by slabs S-200, S-400 and S-600, respectively.

For group III, as shown in Fig. 12, until the failure loads of the slabs, the use of NSM-SHCC plates at both tension and compression sides showed a similar crack width response to that of group II. At crack width of 0.3 mm, the loads carried by slabs STC-200, STC-400 and STC-600, respectively, were 118, 96 and 80 kN, which represent 10, 8 and 7% higher than those obtained by slabs ST-200, ST-400 and ST-600, respectively.

3.7.2. *Deflection-crack width relationship*

The deflection-crack width curves for all slabs are shown in Fig. 13. For group I, as shown in Fig. 13a, increasing the cut-out length increased the measured crack width at the same deflection. For instance, at a deflection of 8.8 mm (allowable service deflection as per ECP-203 [49]), the crack widths of slabs S-200, S-400 and S-600, were about 0.2, 0.27 and 0.40 mm, respectively, these values represent 67, 125 and 233%, respectively, higher than that obtained by the control slab (the crack width was 0.12 mm). This is attributed to the increase in stresses at opening corners with the increase in the opening length. For group II, as shown in Fig. 13b, providing SHCC strips at the tension side, arrested the cracks widening that decreased the crack width readings compared to those of group I. For instance, at a deflection of 8.8 mm, the crack widths of slabs ST-200, ST-400 and ST-600 were about 0.12, 0.16 and 0.20 mm, respectively, these values represent 0, 33 and 67%, respectively, higher than that obtained by the control slab. The slabs of group III showed almost a similar response to that obtained by group II. As shown in Fig. 13c, at a deflection of 8.8 mm, the crack widths of slabs STC-200, STC-400 and STC-600 were about 0.11, 0.16 and 0.19 mm, respectively.

3.8. *Steel strain*

Fig. 14 shows the curves of load versus tensile strain at the continuous steel bar beside the cut-out. The strain of the intermediate steel bar of the control slab was included in the figures for comparison. Based on the material tests of the used high-strength steel bars, the yield strain was 2395 με. As shown in Fig. 14, all slabs showed the yielding of the internal steel reinforcement since the developed strains were greater than the yield value. This observation was matching the mode of failure as all slabs developed a tension failure mode. Comparing the obtained results, it can be observed that the strains on the steel bars of the unstrengthened slabs with cut-outs were relatively higher than that of the control slab SC. As can be seen in Fig. 13a, slabs S-200, S-400 and S-600 reached the yield strain (2395 με) at loads of 97, 79 and 56 kN, respectively, which represent 76, 62 and 44% of that obtained by the control slab SC (127 kN). On the other hand, providing SHCC plates at the tension side of the strengthened slabs of groups II and III showed a decrease in the strain values. As a result, the yielding loads of the strengthened slabs increased. For instance, slab ST-600 reached the yield strain when the load reached about 98 kN which represents 75% higher than that obtained by slab S-600 (56 kN).

4. Prediction of the flexural capacity for the strengthened slabs

As presented in this study, the addition of SHCC plates significantly enhanced the structural performance of the strengthened slabs with cut-outs. Thus, the contribution of the SHCC plates should be considered in the design equations. In the present work, the flexural capacity of the strengthened slabs was predicted based on the equilibrium with assumed full geometric compatibility in the member section. The representation of strains and stresses of the SHCC strengthened section are shown in Fig. 15. The following assumptions were considered for the prediction of the flexural moment:

(1) The ordinary concrete and the SHCC plates were assumed to fail simultaneously in compression,
(2) The maximum strain (ε_{cu}) corresponding to the ultimate compressive stress for concrete can be assumed by 0.003, as per ACI-318 [50],
(3) The tensile strength of ordinary concrete was neglected [45],
(4) The tensile strength provided by the SHCC plates was taken based on the assumptions of JSCE recommendations [52].

Table 5
Test loads corresponding to different crack width (loads in kN).

Group	Slab's designation	at 0.1 mm		at 0.2 mm		at 0.3 mm		at 0.4 mm	
		$P_{0.1}$	WRT SC	$P_{0.2}$	WRT SC	$P_{0.3}$	WRT SC	$P_{0.4}$	WRT SC
Control	SC	70	1.00	100	1.00	120	1.00	132	1.00
Group I	S-200	42	0.60	70	0.70	90	0.75	110	0.83
	S-400	30	0.42	45	0.45	56	0.47	64	0.48
	S-600	24	0.34	32	0.32	38	0.32	40	0.30
Group II	ST-200	57	0.81	87	0.87	107	0.89	128	0.97
	ST-400	45	0.64	69	0.69	89	0.74	106	0.80
	ST-600	35	0.50	55	0.55	75	0.62	92	0.70
Group III	STC-200	60	0.85	101	1.01	118	0.98	131	0.99
	STC-400	48	0.68	75	0.75	96	0.80	115	0.87
	STC-600	36	0.51	55	0.55	80	0.67	100	0.76

$P_{0.1}$ = test load corresponding to crack with of 0.1 mm, $P_{0.2}$ = test load corresponding to crack with of 0.2 mm, $P_{0.3}$ = test load corresponding to crack with of 0.3 mm, $P_{0.4}$ = test load corresponding to crack with of 0.4 mm, WRT SC = with respect to control slab SC.

(5) The steel reinforcement was modeled as elastic-plastic under tension and the maximum strength was limited to the yield strength (f_y) [36,50,55].

The predicted ultimate flexural capacity M_u of the strengthened slabs with cut-outs could be calculated as follows.

$$M_u = T_{st}\left[d - \frac{\alpha\cdot x}{2}\right] + T_P\left[t - \frac{t_P}{2} - \frac{\alpha\cdot x}{2}\right] + C_P\left[\frac{\alpha\cdot x}{2} - \frac{t_P}{2}\right] \quad (3)$$

where

$$C_c = 0.85f'_c[\alpha\cdot x\cdot b - A_{SHCC}] \quad (4)$$

$$C_P = 0.85f'_{c,SHCC}[A_{SHCC} - A_{SP}] + A_{SP}\cdot f_{sc} \quad (5)$$

$$T_{St} = A_s\cdot f_s \quad (6)$$

$$T_P = f_{ty,SHCC}[A_{SHCC} - A_{SP}] + A_{SP}\cdot f_{st} \quad (7)$$

The depth on neutral axis (x) can be obtained based on the equilibrium condition as follows:

$$x = \frac{T_{st} + T_P - C_P + 0.85f'_c\cdot A_{SHCC}}{0.85f'_c\cdot\alpha\cdot b} \quad (8)$$

where

C_c and C_P = the compression forces carried by the concrete and the precast plate, respectively; T_{st} and T_P = the tensile forces carried by tension steel reinforcement and the precast plate; f'_c and $f'_{c,SHCC}$ = the compressive strengths of concrete and SHCC, respectively; $f_{ty,\ SHCC}$ = the SHCC tensile yield strength (First cracking strength as per JSCE recommendations [52]); f_s = the stress in main steel reinforcement; f_{st} and f_{sc} = the stresses of steel reinforcement at SHCC plates at tension and compression sides, respectively; A_{SHCC} and A_{SP} = the plate's cross-sectional and reinforcement areas, respectively; A_s = the area of tension steel reinforcement; b = width of concrete section; d = effective depth of concrete section; t = section total thickness, respectively; α = The stress block factor and taken equals 0.85 in the present study [50].

The experimental and the predicted results are reported in Table 6. As reported in Table 6, the prediction model underestimated the flexural strength of the control slab with a safety margin of 15%. This safety margin decreased with increasing the opening length due to the effect of the stress concentration. The average value of the experimental/analytical results was 1.10 and the coefficient of variation was 0.044.

5. Prediction of maximum crack width

Eurocode2 [56] proposes the following equation for the calculation of the flexural crack width (W_k) of RC members.

$$W_k = S_{r,\max}(\varepsilon_{sm} - \varepsilon_{cm}) \quad (9)$$

The mean tensile strain (ε_{sm}- ε_{sm}) can be obtained by the following equation.

$$(\varepsilon_{sm} - \varepsilon_{cm}) = \frac{(f_s - K_t\left(\frac{f_{cteff}\left(1+n\rho_{eff}\right)}{\rho_{eff}}\right))}{E_s} \geq 0.6\frac{f_s}{E_s} \quad (10)$$

where

f_s = stress in the tension reinforcement assuming cracked section; k_t = 0.6 for short term loading and 0.4 for long term loading; n = the modular ratio $\frac{E_s}{E_{cm}}$, E_s = the design value of the modulus of elasticity of reinforcing steel; E_{cm} = secant modulus of elasticity of the concrete; f_{cteff} = the mean value of concrete tensile strength at which the first crack is expected to occur.

The ratio of tension reinforcement (ρ_{eff}) can be obtained by the following equation.

$$\rho_{eff} = \frac{A_R}{A_{ceff}} \quad (11)$$

where

A_R = area of tension reinforcement and $A_{c,eff}$ = the effective tension area of concrete around the steel reinforcement.

In the current study, when the slabs were provided with precast SHCC plates, the area of tension reinforcement can be obtained by the following equation.

$$A_R = A_s + A_{SHCC}\frac{E_{SHCC}}{E_s} \quad (12)$$

where As = cross-sectional area of steel reinforcement; A_{SHCC} = cross-sectional area of SHCC plate; E_{SHCC} = modulus of elasticity for SHCC material as given in Eq. (13) as per JSCE recommendations [52].

$$E_{SHCC} = 1.77*10^4\sqrt{\frac{\gamma}{18.5}\left(\frac{f_{ck}}{60}\right)^{\frac{1}{3}}} \quad (13)$$

where

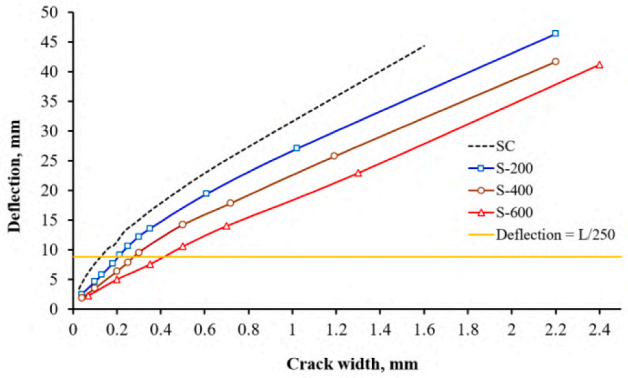
γ = coefficient = 23 [52]; f_{ck} = cylinder compressive strength for SHCC material.

The maximum crack spacing ($S_{r,max}$, mm) is given by the following equation.

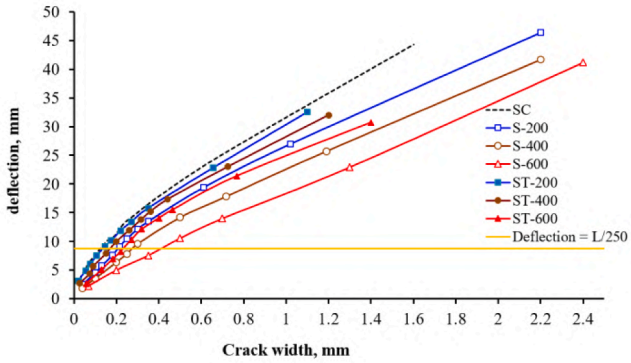
$$S_{r,max} = 3.4c + 0.425k_1k_2\frac{\varnothing}{\rho_{eff}} \quad (14)$$

where

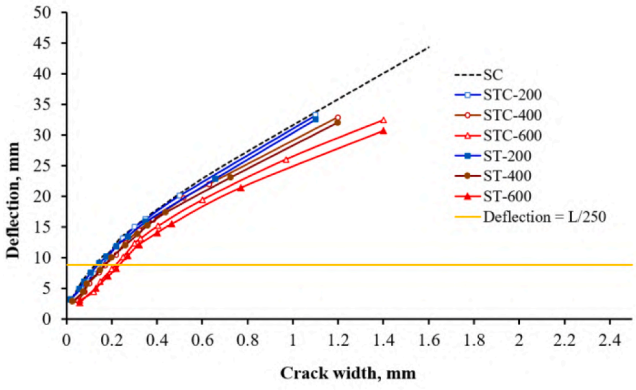
c = clear concrete cover; ∅ = bar diameter; k_1 = coefficient depending upon steel-concrete bond properties and equals to 0.8 for



(a) Curves of slab SC and group I.

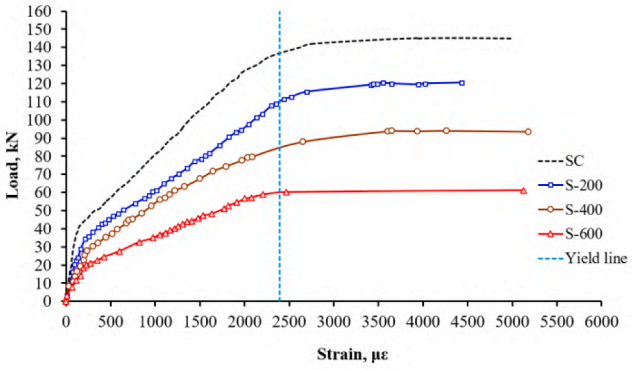


(b) Curves of slab SC, group I and group II.

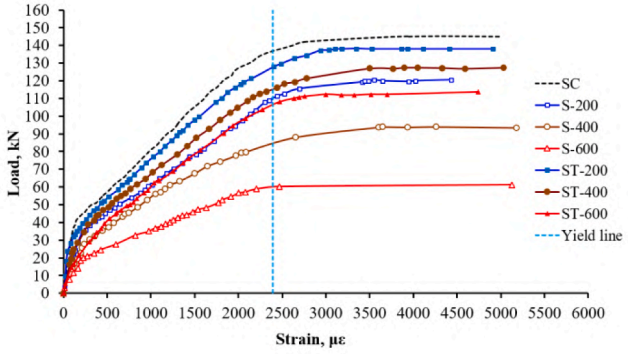


(c) Curves of slab SC, group II and group III.

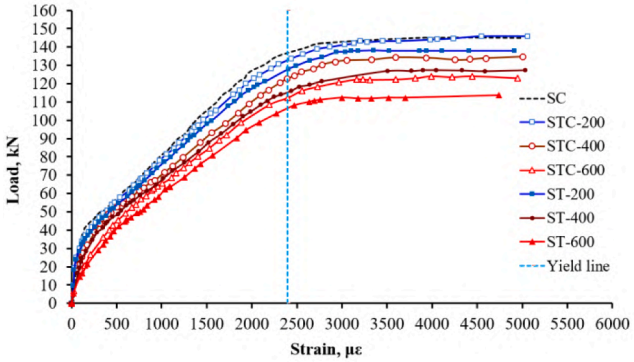
Fig. 13. Deflection-crack width curves of the tested slabs.



(a) Curves of slab SC and group I.



(b) Curves of slab SC, group I and group II.



(c) Curves of slab SC, group II and group III.

Fig. 14. Load strain curves of the tested slabs.

high bond reinforcing bars, and equals to 1.6 for plain reinforcing bars, k_2 = coefficient depending upon loading type and equals to 0.5 for sections subjected to pure bending and equals to 1.0 for sections subjected to pure axial tension.

It is worth mentioning that, Eq. (9) of Eurocode2 was derived for RC members reinforced with steel bars. In spite that Eq. (9) was used for calculating the maximum flexural crack width for the current study pertaining to RC slabs with cut-outs reinforced with steel reinforcement and strengthened with precast SHCC plates. That is to verify the applicability of the equation on the current slabs incorporating some modifications to replace the precast SHCC plates with equivalent steel reinforcement. Table 7 presents the results of the experimental crack widths at service load level and the predicted results based on the proposed model. The service load is defined as the load corresponding to 80% of the yield strain of internal steel reinforcement [50,56]. Comparing the results in Table 7 shows that, the prediction model gave a good prediction for slab SC ($W_{k,exp}/W_{k,predicted} = 1.09$). Whereas for the remaining slabs with cut-outs, the model tends to underestimate the crack width, in addition, the value of $W_{k,exp}/W_{k,predicted}$ increases with increasing the cut-out size. For instance, the values of $W_{k,exp}/W_{k,predicted}$ for slabs ST-200, ST-400 and ST-600 were 1.22, 1.63 and 2.14. This is to be expected as increasing the cut-out size increases the stress concentration at the cut-out corner and this increased the experimental crack width. Accordingly, based on the obtained experimental results of crack width, it is recommended that the Eurocode2 prediction model for crack width should be modified to take into consideration the effect of cut-outs. Based on regression analysis, shown in Fig. 16, the crack width for slabs with cut-outs may be obtained by Eq. (15).

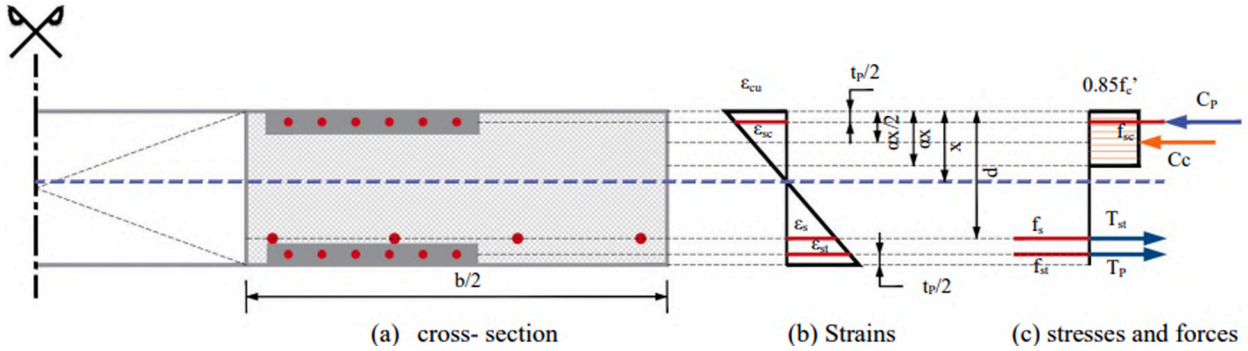


Fig. 15. Strains and stresses of a section strengthened with SHCC plates.

Table 6
Experimental ultimate moments versus predicted results.

Group	Slab's designation	Experimental		Predicted	$M_{u,exp}/M_{u,}$ predicted
		P_u, kN	$M_{u,exp}$, kN.m	$M_{u,predicted}$, kN.m	
Control	SC	145	58.0	50.13	1.15
Group I	S-200	120	48.0	41.77	1.15
	S-400	94	37.6	33.58	1.12
	S-600	67	26.8	25.06	1.07
Group II	ST-200	138	55.2	47.93	1.15
	ST-400	122	48.8	44.83	1.09
	ST-600	105	42.0	39.93	1.05
Group III	STC-200	145	58.0	49.64	1.16
	STC-400	133	53.4	48.93	1.06
	STC-600	124	49.6	47.76	1.03
				Mean	1.10
				SD	0.048
				COV	0.044

P_u = experimental ultimate load; $M_{u,exp}$ = experimental ultimate moment = *0.4* P_u; $M_{u,predicted}$ = predicted flexural moment.

$$W_k = S_{r,max}(\varepsilon_{sm} - \varepsilon_{cm})^*(2.164^*\frac{L_O}{L_S} + 0.911) \quad (15)$$

where

L_O = cut-out (opening) length; L_S = slab width.

The experimental and analytical results for crack width results are presented in Table 7. As shown in Table 7, the modified model gave good results for crack width prediction of the slabs with cut-outs. The mean value of the $W_{k,exp}/W_{k,predicted}$ was 0.98 and the coefficient of variation was 0.04.

6. Conclusion

Based on the carried out experimental program and its results; the following conclusions could be drawn:

- Creation of a cut-out in one-way reinforced concrete slab showed a dramatic decrease in the ultimate capacity, stiffness as well as an increase in the major crack width for the same force. The loss in the ultimate capacity is almost proportional to the increase of the ratio of cut-out length to slab width. For slabs with cut-outs length of 200, 400 and 600 mm, the achieved ultimate loads were 83, 65 and 46% of that achieved by the control slab, respectively.

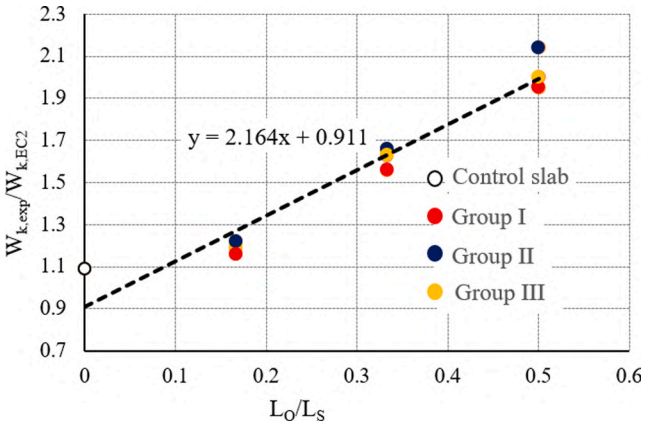


Fig. 16. Relation between L_O/L_s and $W_{k,exp}/W_{k,EC2}$.

Table 7
Experimental crack width versus prediction models.

Group	Slab's designation	Experimental		Predicted by EC2 [56]		Predicted by modified EC2	
		P_s, kN	$W_{k,exp}$, (mm)	$W_{k,predicted}$ (mm)	$W_{k,exp}/W_{k,predicted}$	$W_{k,predicted}$ (mm)	$W_{k,exp}/W_{k,predicted}$
Control	SC	102	0.23	0.21	1.09	–	
Group I	S-200	77	0.25	0.21	1.19	0.26	0.96
	S-400	63	0.35	0.21	1.66	0.34	1.03
	S-600	44	0.41	0.21	1.95	0.42	0.98
Group II	ST-200	97	0.22	0.18	1.22	0.23	0.96
	ST-400	86	0.26	0.16	1.63	0.26	1.00
	ST-600	78	0.30	0.14	2.14	0.28	1.07
Group III	STC-200	98	0.21	0.18	1.16	0.23	0.91
	STC-400	87	0.25	0.16	1.56	0.26	0.96
	STC-600	79	0.28	0.14	2.00	0.28	1.00
				Mean	1.56	Mean	0.98
				SD	0.40		0.04
				COV	0.25		0.04

P_s = service load corresponding to 80% of yield strength of internal steel reinforcement [50,54]; $W_{k,exp}$ = experimental maximum crack width corresponding to service load; $W_{k,predicted}$ = predicted crack width.

- The use of the SHCC plates at the tension side only increased the load-carrying capacities of the slabs with cut-outs to reach about 95, 89 and 95% of that achieved by the control slab for slabs with cut-outs length of 200, 400 and 600 mm, respectively. However, this increase was accompanied by a significant decrease in the ductility. Based on displacement-based ductility, the loss in the ductility factor reached about 58% for the slab with a cut-out length of 600 mm. On the other hand, the application of SHCC plates at both tension and compression sides showed to be a powerful strengthening procedure for restoring the load-carrying capacity with a good ductility performance.
- However, the use of precast SHCC plates at the tension side of slabs with cut-outs showed an insignificant effect on the first flexural crack load, a great improvement in the post cracking behaviour for the strengthened slabs was obtained. Compared to the unstrengthened slabs with cut-outs, the major crack width of the strengthened slab significantly decreased at all load levels. This improvement is owing to the crack arrest action of SHCC material.
- The proposed flexural strength prediction model tends to underestimate the flexural capacity of the strengthened slabs with cut-outs. The average value of the experimental/analytical results was 1.10 and the coefficient of variation was 0.044.
- The prediction model of Eurocode2 gave a good prediction for the maximum crack width of the control slab. While, for the slabs with cut-outs, the model tends to underestimate the crack width value, in addition, the value of $W_{k,exp}/W_{k,predicted}$ increased with increasing the cut-out length. The value of experimental crack width reached about twice the predicted for the slabs with a cut-out length of 600 mm. Accordingly, this study proposed a modification factor for the crack width prediction model of Eurocode2 to suit slabs with cut-outs. The modified model gave good results for the tested slabs with cut-outs; the mean value of $W_{k,exp}/W_{k,predicted}$ was 0.98 and the coefficient of variation was 0.04.

CRediT authorship contribution statement

Abd-Elhakim A. Khalil: Supervision. **Ahmed M. Atta:** Supervision, Conceptualization. **Ali Hassan:** Conceptualization, Data curation, Writing – original draft, Writing – review & editing. **Ahmed A. Henadi:** Data curation.

Declaration of Competing Interest

The authors declare that they have no known competing financial interests or personal relationships that could have appeared to influence the work reported in this paper.

References

[1] Afefy HM, Fawzy TM. Strengthening of RC one-way slabs including cut-out using different techniques. Eng Struct 2013;57:23–36. https://doi.org/10.1016/j.engstruct.2013.09.013.

[2] Al-hafiz AM, Chiad SS, Farhan MS. Flexural strength of reinforced concrete one way opened slabs with and without strengthening. Aust J Basic Appl Sci 2013;7:642–51.

[3] Anil Ö, Kaya N, Arslan O. Strengthening of one way RC slab with opening using CFRP strips. Constr Build Mater 2013;48:883–93. https://doi.org/10.1016/j.conbuildmat.2013.07.093.

[4] Smith ST, Kim SJ. Strengthening of one-way spanning RC slabs with cut-outs using FRP composites. Constr Build Mater 2009;23(4):1578–90.

[5] Bonaldo E, de Barros JA, Lourenço PB. Efficient strengthening technique to increase the flexural resistance of existing RC slabs. J Compos Constr 2008;12(2):149–59.

[6] Bolander JE, Berton S. Simulation of shrinkage induced cracking in cement composite overlays. Cem Concr Res 2004;26(7):861–71.

[7] Barros JA, Cunha VM, Ribeiro AF, Antunes JA. Post-cracking behavior of steel fiber reinforced concrete. Mater Struct 2005;38:47–56.

[8] Walser R, Steiner W. Strengthening a bridge with advanced materials. Struct Eng Int (IABSE) 1997;7(2):110–2.

[9] Almassria B, Halahlab AM. Corroded RC beam repaired in flexure using NSM CFRP rod and an external steel plate. Structures 2020;27:343–51. https://doi.org/10.1016/j.istruc.2020.05.054.

[10] Arslan G, Sevuk F, Ekiz I. Steel plate contribution to load-carrying capacity of retrofitted RC beams. Constr Build Mater 2008;22(3):143–53.

[11] Su RKL, Zhu Y. Experimental and numerical studies of external steel plate strengthened reinforced concrete coupling beams. Eng Struct 2005;27(10):1537–50.

[12] Vasquez A, Karbhari VM. Fiber-reinforced polymer composite strengthening of concrete slabs with cutouts. ACI Struct J 2003;100(5):665–73.

[13] Tan KH, Zhao H. Strengthening of openings in one-way reinforced concrete slabs using carbon fiber-reinforced polymer systems. J Compos Constr, ASCE 2004;8(5):393–402.

[14] Teng JG, Smith ST, Yao J, Chen JF. Intermediate crack induced debonding in RC beams and slabs. Constr Build Mater 2003;17(6-7):447–62.

[15] El-Hacha R, Rizkalla SH. Near-surface-mounted fiber-reinforced polymer reinforcements for flexural strengthening of concrete structures. Struct J 2004;101(5):717–26.

[16] FIB. Externally bonded FRP reinforcement for RC structures – technical report on the design and use of externally bonded fiber reinforced polymer reinforcement (EBR-FRP) for reinforced concrete structures; 2001. 138p.

[17] Hassan T, Rizkalla S. Investigation of bond in concrete structures strengthened with near surface mounted carbon fiber reinforced polymer strips. J Compos Constr 2003;7(3):248–57.

[18] De Lorenzis L, Teng JG. Near-surface mounted FRP reinforcement: an emerging technique for strengthening structures. Compos Part B - Eng 2007;38(2):119–43.

[19] Li M, Li VC. High-early-strength ECC for rapid durable repair: material properties. ACI Mater J 2011;108:3–12.

[20] Zhang Z, Qin F, Ma H, Xu L. Tailoring an impact resistant engineered cementitious composite (ECC) by incorporation of crumb rubber. Construct Build Mater 2020;262:120116.

[21] Li M, Li VC. Cracking and healing of engineered cementitious composites under chloride environment. ACI Mater J 2011;108:333–40.

[22] Zhang Z, Zhang Q. Matrix Tailoring of Engineered Cementitious Composites (ECC) with non-oil-coated, low tensile strength PVA fiber. Construct Build Mater 2018;161:420–31.

[23] Li VC, Wu C, Wang S, Ogawa A, Saito T. Interface tailoring for strain-hardening polyvinyl alcohol-engineered cementitious composite (PVA-ECC). ACI Mater J 2002;99(5):463–72.

[24] Zhang ZG, Hu J, Ma H. Feasibility study of ECC with self-healing capacity applied on long-span steel bridge deck overlay. Int J Pavement Eng 2019;20(8):884–93.

[25] Zhou J, Pan J, Leung CKY. Mechanical behavior of fiber-reinforced engineered cementitious composites in uniaxial compression. J Mater Civ Eng 2015;27(1):04014111. https://doi.org/10.1061/(ASCE)MT.1943-5533.0001034.

[26] Zhang Z, Zhang Q, Li VC. Multiple-scale investigations on self-healing induced mechanical property recovery of ECC. Cem Concr Compos 2019;103:293–302.

[27] Lepech M, Li VC. Durability and long term performance of engineered cementitious composites. Restoration Build Monum 2006;12(2):119–32.

[28] Kojima S, Sakata N, Kanda T, et al. Application of direct sprayed ECC for retrofitting dam structure surface application for mitaka-dam. Concr J 2004;42(5):135–9.

[29] Mündecke E, Mechtcherine V. Tensile behaviour of strain-hardening cement-based composites (SHCC) with steel reinforcing bars. Cem Concr Compos 2020;105:103423. https://doi.org/10.1016/j.cemconcomp.2019.103423.

[30] Li J, Weng J, Yang E-H. Stochastic model of tensile behavior of strain-hardening cementitious composites (SHCCs). Cem Concr Res 2019;124:105856. https://doi.org/10.1016/j.cemconres.2019.105856.

[31] Fischer G, Li V. Influence of matrix ductility on tension-stiffening behavior of steel reinforced engineered cementitious composites (ECC). ACI Struct J 2002;99(1):104–11.

[32] Rokugo K, Lim SC, Kanda T, Kunieda M, Fujimoto Y. Tensile behavior of ECC members with or without reinforcement. In: Proc. of International RILEM Workshop on HPFRCC in Structural Applications; 2005. p. 279–86.

[33] Kunieda M, Hussein M, Ueda N, Nakamura H. Enhancement of crack distribution of UHP-SHCC under axial tension using steel reinforcement. J Adv Concr Technol 2010;8(1):49–57.

[34] Li VC. On engineered cementitiouscomposities (ECC), a review of the material and its applications. J Adv Concr Technol 2003;1:215–30.

[35] Li VC, Fischer G. Reinforced ECC – an evolution from materials to structures. In: Proceedings on CD, Session 5, Paper K-13, Fib 2002, Osaka, Japan; 2002.

[36] Khalil A, Etman E, Atta A, Essam M. Behavior of RC beams strengthened with strain hardening cementitious composites (SHCC) subjected to monotonic and repeated loads. Eng Struct 2017;140:151–63. https://doi.org/10.1016/j.engstruct.2017.02.049.

[37] Hassan A, Baraghith AT, Atta AM, El-Shafiey TF. Retrofitting of shear-damaged RC T-beams using U-shaped SHCC jacket. Eng Struct 2021;245:112892. https://doi.org/10.1016/j.engstruct.2021.112892.

[38] Afefy HM, Kassem NM, Mahmoud MH, Taher S-D. Efficient strengthening of opened-joint for reinforced concrete broken slabs. Compos Struct 2016;136:602–15.

[39] Afefy HM, Kassem NM, Hussein M. Enhancement of flexural behavior of CFRP-strengthened reinforced concrete beams using engineered cementitious composites transition layer. Struct Infrastruct Eng 2015;UK 11(8):1042–53.

[40] Hussein M, Kassem NM, Hassan A. An Innovative Efficient Strengthening For Reinforced Low Strength Concrete Cantilever Slabs. IOSR-JMCE 2015; volume 12, issue 5 Ver. I, PP 01-13; 2015.

[41] Kassem M, El-Shafeiy T, Hussein M, Afefy H, Hassan A. Shear Behaviour of SHCC Dry Joints in Precast Construction International Conference on Advances in Structural and Geotechnical Engineering, ICASGE'17, Hurghada, Egypt, 27–30 March 2017.
[42] Zhang J, Gao Y, Wang Z. Evaluation of shrinkage induced cracking performance of low shrinkage engineered cementitious composite by ring tests. Compos Part B 2013;52:21–9.
[43] Neville AM. Properties of concrete, 3rd ed., Pitman Publishing Limited; 1981.
[44] Li M, Li VC. Behavior of ECC/concrete layer repair system under drying shrinkage conditions. In: Proceedings of ConMat'05, Vancouver, Canada, August; 2005. p. 22–4.
[45] Yang EH, Yang Y, Li VC. Use of high volumes of fly ash to improve ECC mechanical properties and material greenness. ACI Mater J 2007;104(6):303–11.
[46] Afefy H-D, Mahmoud MH. Structural performance of RC slabs provided by pre-cast ECC strips in tension cover zone. Constr Build Mater 2014;65:103–13.
[47] Hassan A, Atta AM, El-Shafiey TF. Restoration of the shear capacity for RC beams with web openings using precast SHCC plates. Structures 2020;25:603–12. https://doi.org/10.1016/j.istruc.2020.03.046.
[48] Afefy HM, Baraghith AT, Hassan A, Abuzaid MK. Strengthening of shear-deficient RC beams using near surface embedded precast cement-based composite plates (PCBCPs). Eng Struct 2021;244:112765. https://doi.org/10.1016/j.engstruct.2021.112765.
[49] Egyptian code for design and construction of reinforced concrete structures (ECP 203-2020); 2020.
[50] ACI Committee 318 (2019). Building Code Requirements for Structural Concrete (ACI 318-19) and Commentary (ACI 318R-19). American Concrete Institute, Farmington Hills, MI, 519 pp.
[51] Li VC. Tailoring ECC for special attributes: a review. Int J Concr Struct Mater 2012;6(3):135–44.
[52] Japan Society of Civil Engineers (JSCE). Recommendations for design and construction of high performance fiber reinforced cement composite with multiple fine cracks (HPFRCC), Concrete engineering series 82; 2008.
[53] Hussein M, Kunieda M, Nakamura H. Strength and ductility of RC beams strengthened with steel-reinforced strain hardening cementitious composites. Cem Concr Compos 2012;34(9):1061–6. https://doi.org/10.1016/j.cemconcomp.2012.06.004.
[54] CEB-FIP. Model code for concrete structures: CEB-FIP international recommendations. Paris: Comite Euro-International du Beton; 2010. p. 312.
[55] Zhang Y, Li X, Zhu Y, Shao X. Experimental study on flexural behavior of damaged reinforced concrete (RC) beam strengthened by toughness-improved ultra-high performance concrete (UHPC) layer. Compos B 2020;186:107834. https://doi.org/10.1016/j.compositesb:2020.107834.
[56] EN 1992-1-1. Eurocode 2: design of concrete structures – Part 1-1: general rules and rules for buildings. Brussels: European Committee for Standardization (CEN); December 2004.